Effect of metal ions on the internal motions of Adenylate Kinase: A Molecular dynamics simulation study

Marzieh Allahdaneh[1], Emran Heshmati[*1] and Khosrow Khalifeh[1*]

1- Department of Biology, Faculty of science, University of Zanjan, Zanjan, Iran.

[*]Correspondence to: Emran Heshmati, heshmati@znu.ac.ir and Khosrow Khalifeh, khalifeh@znu.ac.ir Department of Biology, Faculty of science, University of Zanjan, University Blvd, Zanjan-Iran. Tel: +982433052531 Fax: +982433052543

Short title/running title: Effect of metal ions on Adenylate Kinase dynamics

Abstract

Adenylate Kinase (ADK) catalyzes the reversible interconversion between cytoplasmic nucleotides that is essential for energy homeostasis. We performed several Molecular Dynamics simulations on ADK, containing metal ions Mg^{+2} and Zn^{+2}. The dynamics of the enzyme were computed on the ion-free structure, and the structures containing individual ions. RMSD and Rg data demonstrate that the coordination of Zn^{+2} does not significantly affect the overall stability of the enzyme. Decreasing the overall dynamics of the enzyme in the presence of both metal ions was explained by the cooperativity between the stabilizing interactions of metal ions. The high RMSF value of a specific segment in the presence of both ions, demonstrates that a fine balance between the conformational stability and local structural dynamics may be involved in the regulation of the enzyme catalysis. It was also concluded that the orientation of the structural domains is affected by the simultaneous presence of both ions.

Keywords: Adenylate Kinase, Molecular Dynamics, metal ion, stability, catalytic activity

Introduction:

Adenylate kinase (ADK), also known as myokinase (EC: 2.7.4.3), is a ubiquitous phosphoryl-transfer enzyme found from bacteria to eukaryotes. ADK catalyzes the reversible phosphoryl transferal reaction (ATP +AMP ↔ ADP+ADP). The reversible nature of the reaction, indicates that the enzyme is central to the energy balance of all organisms by stablishing the equilibrium between cytoplasmic nucleotides [1].

Structurally, ADK is composed of three distinct domains, including ATP binding that is known as LID (residues 118-160), AMP binding region known as NMP domain (residues 30-67), and

the core structure including residues 1-29, 68-117, and 161-214[2]. It was shown that during substrate hydrolysis, it undergoes a large-scale structural switch from open to closed conformation [3–5]. A magnesium cofactor is coordinated in the active site pocket by electrostatic interactions, and is required for the enzyme's activity. It was shown that Mg^{2+} operates as the activating ion leading to the formation of the MgATP and MgADP complexes that function as substrates for the phosphoryl-transfer reaction [1,6].

From a quantum mechanical point of view, the enzyme-catalyzed reactions are performed under a delicate balance between the stability and dynamics of the enzyme structure. For ADK, the coupling between stability and flexibility, especially at the active site of the enzyme is critical for structural changes from open to closed and to facilitate substrate hydrolysis [3,7]. The dynamics of different variants of ADKs were intensively investigated by experimental and computational tools [4,8–16].

Computer simulations of experimentally NMR spectra for porcine ADK demonstrated that Mg^{+2} ion has a critical role in the differentiation of the two nucleotide-binding sites on adenylate kinase [8]. To explain the way of substrate binding on the catalytic center of ADK during each reaction cycle, the induced-fit motion model was proposed [9]. By comparing the crystal structure of substrate-free adenylate kinase from Escherichia coli and the same enzyme complexed with an inhibitor mimicking, ATP and AMP; Muller et al. showed that the chain mobility of the enzyme in a region far from the active site center increases upon substrate binding. They concluded that the energy of substrate binding is required for specificity [4]. Domain closure of ADK was investigated using the time-resolved dynamic excitation energy transfer (ET), and it was shown that the enzyme undergoes a two-step domain closure and that the multiple conformations of E. coli ADK are present in solution at equilibrium conditions [11]. In a comparative study by Nuclear

Magnetic Resonance (NMR) spectroscopy on hyperthermophile and mesophilic homologs of ADK, Wolf-Wats et al. showed that catalysis involves domain rearrangements. They also reported that the coupling of stability and functional dynamics of the substrate-enzyme complex allows the enzymes to perform the same catalysis reaction in organisms with different environmental conditions [3]. High-resolution single-molecule FRET studies on ADK demonstrated that it dynamically samples two distinct states, where the equilibrium favors the closed state even in the absence of substrates. They explained that the interaction with substrates leads to increasing the closing rate of the lid and restriction of the conformational dynamics [12]. Molecular dynamics simulations and experimental evidences indicate that partially and fully closed conformations are sampled in nanoseconds and microsecond-to-millisecond timescales; respectively. It was also shown that larger-scale motions in substrate-free ADK directionally and non-randomly follow the pathways toward the formation of functional conformation [13].

The dynamics of the ATP/AMP lid and the core domain of ADK were described as hierarchical clustering of fluctuations using MD simulation studies, and it was shown that dynamics of the protein could be described as a set of hierarchically rigid-domain pairs along with associated inter-domain fluctuations [14]. Recent bioinformatics and MD simulation studies demonstrated that the evolution of psychrophilic, mesophilic and thermophile variants of closely related ADKs are in good agreement with the changes that occurred in the environmental conditions of the globe during evolutionary time-scale. It was also proposed that different dynamic behavior of the ADKs is due to the presence of two flexible regions, so that a fine balance between the flexibility of these fragments help protein variants to act at their operating temperatures [16].

In current work, an MD simulation study was performed on the mesophilic variant of ADK (PDB ID: 1P3J) in the presence and absence of Mg^{+2} and Zn^{+2}. The experimental structure of ADK for this study is in closed state.

2. Materials and methods

The starting structure for the MD simulation was X-ray resolved crystal structure of adenylate kinase (ADK) from *bacillus subtilis* obtained from Protein Data Bank (PDB ID: 1p3j, resolution of 1.9 Å) [17]. The structure contains 217 residues, metal ions magnesium (Mg^{+2}) and zinc (Zn^{+2}) as well as AP5 as ligands. Four structural models that were subjected to MD simulation include ion-free structure ($Mg^{o}Zn^{o}$) and structures containing Mg^{+2} ($Mg^{*}Zn^{o}$), Zn^{+2} ($Mg^{o}Zn^{*}$) and both ions ($Mg^{*}Zn^{*}$). All simulations was performed at 300 K, using standard MD under AMBER force field, [18]implemented in the Gromacs software packages, version 5.1.2 [19,20]

Simulation box with a rhombic dodecahedron shape containing 2.0 nm distances between periodic images was used for simulation. The protein structures with/without ions were solvated in periodic boundary conditions and the SPC/E water model.

PROPKA software (under the PDB2PQR 7package) [21] was used to set the protonation state of ionizable side-chains as well as the N- and C- termini according to pKa values of isolated side-chain groups at pH=7, and then appropriate numbers of Cl^{-} and Na^{+} ions were added to each system to neutralize the total charge of the systems similar to the physiologic ionic condition (100 mM). To remove any steric clashes or inappropriate geometry, the systems were energetically minimized for maximum of 5000 steps, and the solvent and ions around the protein were equilibrated via an NVT (canonical) followed by an NPT simulation (P=1 atm), each consist of 100 ps simulation time.

Berendsen algorithm [22] was used to maintain constant-temperature and pressure, and the particle mesh Ewald (PME) algorithm was used for setting the long-range interactions [23]. Short-range electrostatic and Van der Waals interactions were calculated with a distance cut-off of 1.0 nm. After equilibration, any system was subjected to molecular dynamics simulations for 100 ns with 2.0 fs time step using the above mentioned simulation parameters.

The aim of this study is the investigation of the dynamic of ADK at different states of ionic conditions regarding the presence and/or absence of Mg^{+2} and Zn^{+2} ions. To that end, the dynamic parameters including, the time-dependent radius of gyration (Rg), the root mean square deviations (RMSD), and root mean square fluctuations (RMSF) of backbone atom positions from starting structures were calculated and compared. Finally, the time-dependent distance of Zn^{+2} and Mg^{+2} ions from all residues of the structures were calculated and compared.

3. Results and discussion

3.1 Description of the structure of ADK

Conformational dynamics of the enzymes, originated from their internal motions, plays an essential role in their catalysis. Molecular Dynamics (MD) simulation on the enzymes can provide the atomistic detail concerning time-dependent behavior motions at the individual residues. On the other hand, the activity of the ADK is regulated by a delicate balance between the stability and structural dynamics of the enzyme. To understand the atomistic details of the effect of metal ions on the internal motions of the enzyme, MD simulations were performed on the enzyme in its original crystal structure ($Mg^{*}Zn^{*}$) as well as the ion-free structure ($Mg^{o}Zn^{o}$), and the structures containing individual ions ($Mg^{*}Zn^{o}$ and $Mg^{o}Zn^{*}$). The closed conformation of the ADK (PDB ID: 1p3j) is shown in Fig. 1A & B. The structure contains metal ions Mg^{+2} and

Zn^{+2}, and distinct regions of the enzyme, including the LID domain, NMP domain, and the core structure, are shown by the color scheme (Fig 1A). Examining the structure of ADK (Fig. 1B) indicates that the ligand has more stabilizing interaction with the LID domain compared with the NMP and the core domain of the enzyme. It can also be seen that four residues in the LID domain are involved in the coordination of Zn^{+2} ion. Based on this observation, it is expected that the LID region may has a critical role in the stability of the ADK complex in the closed functional conformation.

Fig. 1.

3.2 RMSD and Rg

Analysis of MD simulations were initiated by RMSD calculation to evaluate the overall stability of the enzyme at different conditions regarding the presence or absence of metal ions. To ensure complete equilibration of the system, the analysis was done on the final 30 ns of the simulation time (70-100 ns). The time-dependent RMSD for the structures are shown in Fig. 2A.

Fig. 2.

Comparing the results of the RMSD values shows that the behavior of the structures in ion-free structure and in the structure containing Zn^{+2} is approximately the same, indicating that the coordination of Zn^{+2} does not significantly affect the RMSD. However, Mg^{+2} decreases the overall fluctuation of the enzyme, and the most reduction in the RMSD is observed in the structure containing both metal ions. This observation can be attributed to the position of metal ions in the structure of the protein and their ability to create short and long electrostatic interactions (Fig. 1). The enzyme contains 40 residues of negatively and 26 residues of positively

charged amino acids that are distributed in the structure of the protein. On the other hand, the Zn^{+2} is a surfaced-exposed element that is surrounded by flexible loops. The effective dielectric constant in this region is higher than that in the interior and hydrophobic regions of the protein. Accordingly, the strength of the electrostatic interaction between Zn^{+2} and nearby residues of the loops is low compared with the corresponding force stablished by Mg^{+2} ion. These observations demonstrate that the simultaneous occurrence of both ions has a cooperativity effect that results in more reduction of the RMSD value. The changes in the Rg values for the structures are provided in Fig. 2B. From Fig. 2B, moderate Rg value is observed in the presence of both ions. Also, it can be seen that the Rg of the ion-free enzyme is higher in comparison to other structures, and the inclusion of Mg^{+2} to the structure leads to decreasing the Rg of the corresponding structure. It was also revealed that the Rg of the protein structure undergoes more fluctuation in the presence of Zn^{+2}. Since the Rg is a reflection of the compactness of the protein, it can be said that the presence of two ions in the structure, cooperatively increases the stabilizing interactions that lead to a reduction in Rg value. In the absence of Mg^{+2}, and elimination of the cooperativity, the interaction of Zn^{+2} with the flexible loops is weekend, and more fluctuation is observed in the Rg values.

3.3 RMSF

Considering distinct positions of the metal ions in the tertiary structure of the enzyme, it is expected that they have various structural effects on different regions of the protein. To investigate the positional effects of the metal ions on the flexibility of protein structure, RMSF values were calculated, and the results of the final 30 ns are shown in Fig. 3. For clarity, data are presented in a specific format, where the structures could be separately compared with the ion-free enzyme as the reference structure.

Fig. 3.

The previous investigation has been shown that ADK has two main flexible regions that are coincident with the LID and NMP domains [16]. Hence, it is expected that these regions are affected by metal ions under our simulation conditions. Comparison of the RMSF values of Fig. 3A & B shows that the effect of Zn^{+2} on the fluctuation of residues is lower than that from Mg^{+2}. Furthermore, it can be seen that the flexibility of two regions, including residues 30-50 from the LID domain as well as residues 157-178 of the core domain, are affected by Zn^{+2}. While, the effect of Mg^{+2} is extended to the whole structure of the enzyme toward decreasing the flexibility. Since the coordination of Zn^{+2} occurs at the LID domain in the margin of the protein structure, its positional effects are restrained to this region. On the other hand, the electrostatic interactions of the Mg^{+2} in the core structure of the protein with a low dielectric constant can be extended to the whole structure of the enzyme. According to Fig. 3C, the simultaneous occurrence of both ions in the structure of the protein, has interesting consequences on the dynamics of the representative flexible regions of the protein structure. Fig. 3C shows that the flexibility of fragment 36-57 in the first flexible region increases; while, it has a dual effect of the second flexible region of the structure in which the flexibility of the fragment 126-144 decreases, and that for the fragment 145-149 increases. Increasing the flexibility of the fragment 36-57 in NMP domain in the presence of both ions demonstrates that this condition is essential in the regulation of the catalytic activity of the enzyme.

Time dependent residue-ion distance

Three-dimensional space around metal ions were subjected to more detailed examination by calculation of the time-dependent minimum distance of individual ions from all residues in the tertiary structure of the enzyme. Fig. 4A shows the minimum distance of Mg^{+2} from the protein

residues with and without Zn^{+2}. The corresponding distance parameter for Zn^{+2} with and without Mg^{+2} is also provided in Fig. 4B.

Figure 4.

Mg^{+2} is located in the active site of the enzyme (Fig. 1) and is involved in transferase reaction via binding to ATP. As shown in Fig. 4A, upon coordination of Zn^{+2} in the structure of the protein, the distance of the fragment 136-144 from Mg^{+2} increases, and that of the fragments 128-135 and 154-175 decreases. Previous studies have shown that the binding site for ATP is created from the interaction of the central and LID domains. Since residues 136-144 and 128-135 are located in the context of the LID domain, it can be concluded that coordination of Zn^{+2} results in local rearrangement of the LID structure to provide conditions for ATP-binding at the active site. Since the fragment 154-157 belongs to the core domain of the protein, changing its distance from the Mg^{+2}, demonstrate that Zn^{+2} could also influence the ATP binding site in a long-range manner. The distances of the Mg^{+2} with the critical residues in the presence and absence of Zn^{+2} are provided in Table 1.

Table. 1.

The Zn^{+2} is coordinated by residues Cyc130, Cys133, Cyc150, and Asp153 (Fig. 1). Fig. 4B shows the distance of all residues with the Zn^{+2} in the absence and presence of Mg^{+2}. As expected, the minimum distance of Zn^{+2} in both structures is observed for the fragments 130-133 and 150-153. On the other hand, the coordination of Mg^{+2} does not affect the local tertiary structure around Zn^{+2}. However, the presence of Mg^{+2} reduces the distance of Zn^{+2} with the fragment 10-25; and increases its distance with fragment 50-118. The latter segment covers parts of the NMP and the core domains of the enzyme. Hence, it seems that the Zn^{+2} provide structural conditions for the interaction of these domains for AMP-binding.

Conclusion

The LID and NMP domains of ADK have intrinsically flexible regions that are affected by the coordination of metal ions. The simultaneous presence of Mg^{+2} and Zn^{+2} unexpectedly leads to increasing the dynamics of the second flexible region at the catalytic site. The presence of the ions could also affect the structural rearrangement of the LID and core domains of the enzyme. Hence, it seems that the local justification of the dynamics by metal ions may have a critical role in the regulation of the enzyme catalysis.

References

1. Knowles, J. R. Enzyme-Catalyzed Phosphoryl Transfer Reactions. *Annu. Rev. Biochem.* **1980**, *49*, 877–919. https://doi.org/10.1146/annurev.bi.49.070180.004305.

2. Wang, J.; Peng, C.; Yu, Y.; Chen, Z.; Xu, Z.; Cai, T.; Shao, Q.; Shi, J.; Zhu, W. Exploring Conformational Change of Adenylate Kinase by Replica Exchange Molecular Dynamic Simulation. *Biophys. J.* **2020**, *118*, 1–10. https://doi.org/10.1016/j.bpj.2020.01.001.

3. Wolf-Watz, M.; Thai, V.; Henzler-Wildman, K.; Hadjipavlou, G.; Eisenmesser, E. Z.; Kern, D. Linkage between Dynamics and Catalysis in a Thermophilic-Mesophilic Enzyme Pair. *Nat. Struct. Mol. Biol.* **2004**, *11* 10, 945–949. https://doi.org/10.1038/nsmb821.

4. Müller, C. W.; Schlauderer, G. J.; Reinstein, J.; Schulz, G. E. Adenylate Kinase Motions during Catalysis: An Energetic Counterweight Balancing Substrate Binding. *Structure* **1996**, *4*, 147–156. https://doi.org/10.1016/S0969-21269600018-4.

5. Müller, C. W.; Schulz, G. E. Structure of the Complex between Adenylate Kinase from Escherichia Coli and the Inhibitor Ap5A Refined at 1.9 Å Resolution. A Model for a

Catalytic Transition State. *J. Mol. Biol.* **1992**, *224*, 159–177. https://doi.org/10.1016/0022-28369290582-5.

6. Morrison, J. F.; Uhr, M. L. The Function of Bivalent Metal Ions in the Reaction Catalysed by ATP: Creatine Phosphotransferase. *BBA - Enzymol. Biol. Oxid.* **1966**, *122*, 57–74. https://doi.org/10.1016/0926-65936690091-9.

7. Kerns, S. J.; Agafonov, R. V.; Cho, Y. J.; Pontiggia, F.; Otten, R.; Pachov, D. V.; Kutter, S.; Phung, L. A.; Murphy, P. N.; Thai, V.; et al. The Energy Landscape of Adenylate Kinase during Catalysis. *Nat. Struct. Mol. Biol.* **2015**, *22* 2, 124–131. https://doi.org/10.1038/nsmb.2941.

8. Vasavada, K. V.; Kaplan, J. I.; Rao, B. D. N. Analysis of 31P NMR Spectra of Enzyme-Bound Reactants and Products of Adenylate Kinase Using Density Matrix Theory of Chemical Exchange. *Biochemistry* **1984**, *23*, 961–968. https://doi.org/10.1021/bi00300a025.

9. Schulz, G. E. Induced-Fit Movements in Adenylate Kinases. *Faraday Discuss.* **1992**, *213*, 627–630. https://doi.org/10.1039/FD9929300085.

10. Berry, M. B.; Meador, B.; Bilderback, T.; Liang, P.; Glaser, M.; Phillips, G. N. The Closed Conformation of a Highly Flexible Protein: The Structure of E. Coli Adenylate Kinase with Bound AMP and AMPPNP. *Proteins Struct. Funct. Bioinforma.* **1994**, *19* 3, 183–198. https://doi.org/10.1002/prot.340190304.

11. Sinev, M. A.; Sineva, E. V.; Ittah, V.; Haas, E. Domain Closure in Adenylate Kinase. *Biochemistry* **1996**, *35*, 6425–6437. https://doi.org/10.1021/bi952687j.

12. Hanson, J. A.; Duderstadt, K.; Watkins, L. P.; Bhattacharyya, S.; Brokaw, J.; Chu, J. W.; Yang, H. Illuminating the Mechanistic Roles of Enzyme Conformational Dynamics. *Proc. Natl. Acad. Sci. U. S. A.* **2007**, *104*, 18055–18060. https://doi.org/10.1073/pnas.0708600104.

13. Henzler-Wildman, K. A.; Thai, V.; Lei, M.; Ott, M.; Wolf-Watz, M.; Fenn, T.; Pozharski, E.; Wilson, M. A.; Petsko, G. A.; Karplus, M.; et al. Intrinsic Motions along an Enzymatic Reaction Trajectory. *Nature* **2007**, *450*, 838–844. https://doi.org/10.1038/nature06410.

14. Moritsugu, K.; Koike, R.; Yamada, K.; Kato, H.; Kidera, A. Motion Tree Delineates Hierarchical Structure of Protein Dynamics Observed in Molecular Dynamics Simulation. *PLoS One* **2015**, *10* 7, 1–13. https://doi.org/10.1371/journal.pone.0131583.

15. Chen, Y. L.; Habeck, M. Data-Driven Coarse Graining of Large Biomolecular Structures. *PLoS One* **2017**, *12* 8, 1–17. https://doi.org/10.1371/journal.pone.0183057.

16. Mohamadnejhadi, H.; Beiramzadeh, A.; Shadman Lakmehsari, M.; Khalifeh, K.; Heshmati, E. Temperature Dependent Dynamics in Highly Homologous Adenylate Kinases. *J. Biomol. Struct. Dyn.* **2019**, *38* 7, 1–24. https://doi.org/10.1080/07391102.2018.1477622.

17. Bae, E.; Phillips, G. N. Structures and Analysis of Highly Homologous Psychrophilic, Mesophilic, and Thermophilic Adenylate Kinases. *J. Biol. Chem.* **2004**, *279* 27, 28202–28208. https://doi.org/10.1074/jbc.M401865200.

18. Duan, Y.; Wu, C.; Chowdhury, S.; Lee, M. C.; Xiong, G.; Zhang, W.; Yang, R.; Cieplak, P.; Luo, R.; Lee, T.; et al. A Point-Charge Force Field for Molecular Mechanics

Simulations of Proteins Based on Condensed-Phase Quantum Mechanical Calculations. *J. Comput. Chem.* **2003**, *24* 16, 1999–2012. https://doi.org/10.1002/jcc.10349.

19. Hess, B.; Kutzner, C.; Van Der Spoel, D.; Lindahl, E. GRGMACS 4: Algorithms for Highly Efficient, Load-Balanced, and Scalable Molecular Simulation. *J. Chem. Theory Comput.* **2008**, *4* 3, 435–447. https://doi.org/10.1021/ct700301q.

20. Van Der Spoel, D.; Lindahl, E.; Hess, B.; Groenhof, G.; Mark, A. E.; Berendsen, H. J. C. GROMACS: Fast, Flexible, and Free. *Journal of Computational Chemistry*. 2005, pp 1701–1718. https://doi.org/10.1002/jcc.20291.

21. Dolinsky, T. J.; Nielsen, J. E.; McCammon, J. A.; Baker, N. A. PDB2PQR: An Automated Pipeline for the Setup of Poisson-Boltzmann Electrostatics Calculations. *Nucleic Acids Res.* **2004**, *32* WEB SERVER ISS.. https://doi.org/10.1093/nar/gkh381.

22. Berendsen, H. J. C.; van der Spoel, D.; van Drunen, R. GROMACS: A Message-Passing Parallel Molecular Dynamics Implementation. *Comput. Phys. Commun.* **1995**, *91* 1–3, 43–56. https://doi.org/10.1016/0010-46559500042-E.

23. Darden, T.; York, D.; Pedersen, L. Particle Mesh Ewald: An N·logN Method for Ewald Sums in Large Systems. *J. Chem. Phys.* **1993**, *98*, 10089. https://doi.org/10.1063/1.464397.

Table and figures legends:

Table. 1. The Distance (Mean ± SD) of representative residues from Mg+2 after equilibration, in comparison with those in crystal structure.

Fig. 1. Graphical representation of ADK. (A) The overall tertiary structure of the protein, including three distinctive domains, are shown in the ribbon diagram in different colors. Metal ions Zn+2 (red circle) and Mg+2 (magenta circle) are also shown in their positions. (B) Closed-

up view of the various residues from different regions of the protein that are involved in the interaction with the ligand and metal ion coordination are shown. The graphical manipulation of the structure (PDB ID: 1p3J) was done with the Chimera program.

Fig. 2. The RMSD and Rg plots generated from molecular dynamics simulations (A) RMSD of ADK at various conditions of metal ions during the final 30 ns of the simulation time (B) Rg values at different states of metal ions during the last 30 ns of the simulation time.

Fig. 3. RMSF plot generated from molecular dynamics simulations. (A) RMSF values of ADK without metal ions and with Zn+2. (B) RMSF values of ADK without metal ions and with Mg^{+2}. (C) RMSF values of ADK without metal ions and with Zn^{+2} and Mg^{+2}.

Figure 4. Residues distances from the metal ions. (A) Comparison of the residue distance from Mg+2 in the absence and presence of Zn+2. (B) comparison of the residue distance from Zn+2 in the absence and presence of Mg+2.

. Table. 1.

Residue	Distance (Å)		
	Crystal structure	Simulated structures	
		Mg* Zn^{o}	Mg* Zn*
Gly14	4.27	5.32±0.42	6.71±1.48
Glu18	10.28	8.37±0.65	9.21±1.09
His28	10.55	6.23±0.30	6.45±0.36
Ser30	6.82	3.97±0.14	3.86±0.11
Asp33	6.85	4.30±0.10	4.31±0.09
Met34	10.33	8.58±0.45	8.27±0.42
Arg36	10.71	8.68±0.64	9.38±0.59
Asp84	7.13	3.90±0.17	3.99±0.08
Arg88	12.57	13.79±0.55	11.79±0.78
Phe141	15.93	14.75±2.39	24.79±0.99
Arg160	10.78	21.17±0.90	10.29±1.36
Asp162	11.92	19.48±0.76	8.42±1.32
Arg171	12.53	16.33±0.72	11.20±1.32

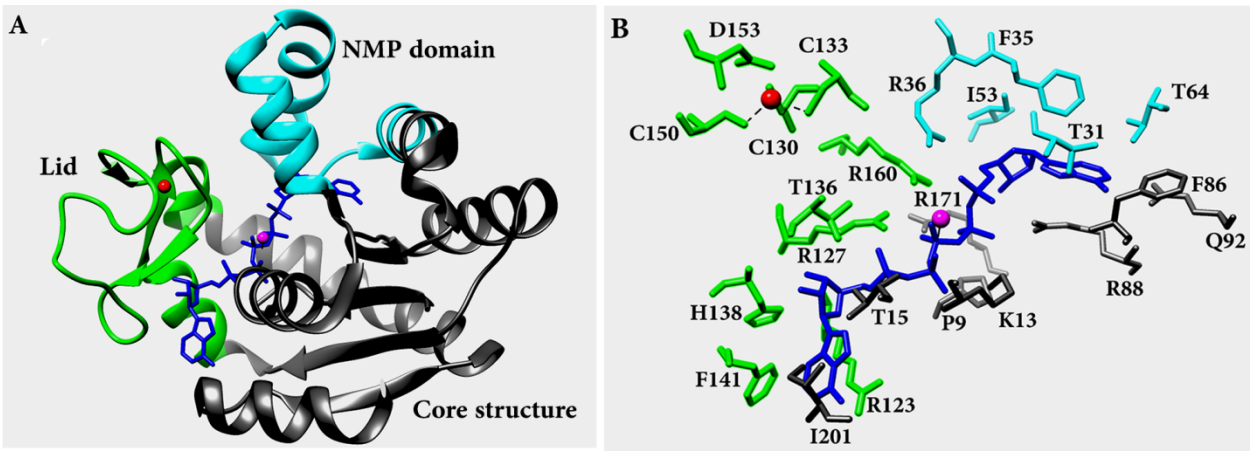
A
NMP domain
Lid
Core structure
B
D153
C133
F35
R36
I53
T64
C150
C130
T31
R160
T136
R171
F86
R127
Q92
R88
H138
T15
P9
K13
F141
R123
I201

Fig. 1.

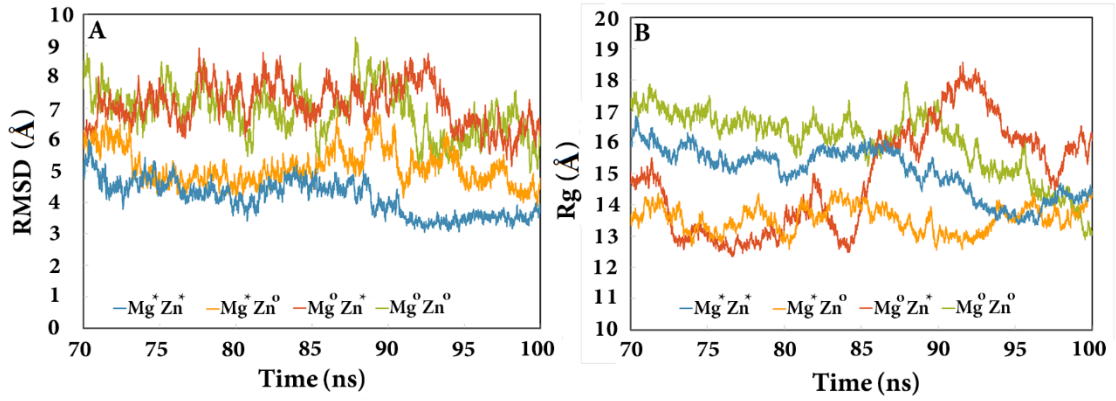
A
RMSD (Å)
Time (ns)
B
Rg (Å)
Time (ns)
Mg* Zn*
Mg* Zn°
Mg° Zn*
Mg° Zn°

Fig. 2.

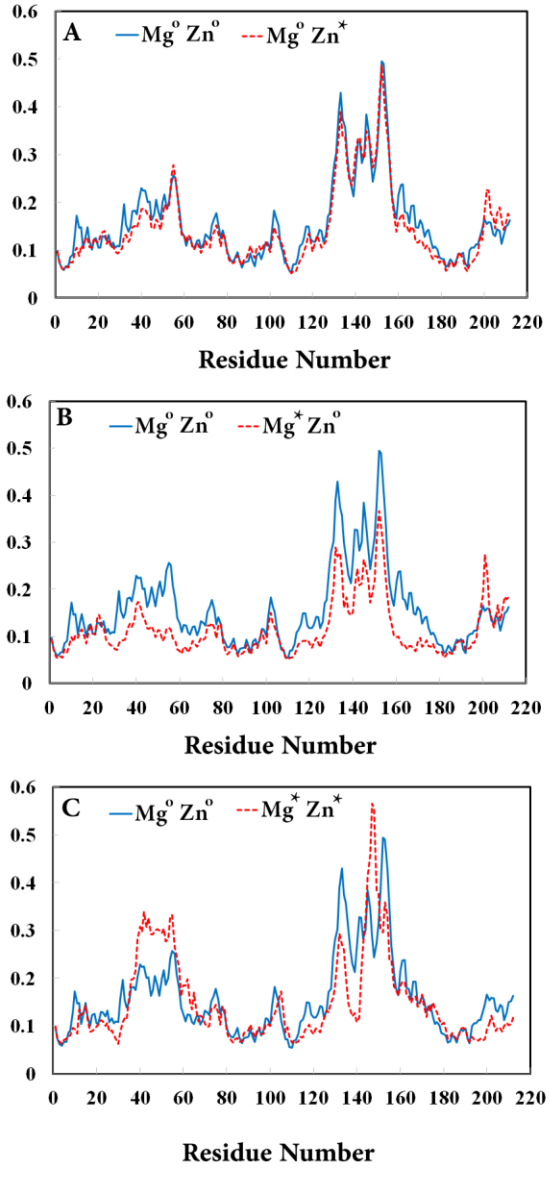
A
Mg° Zn°
Mg° Zn*
0.6
0.5
0.4
0.3
0.2
0.1
0
0 20 40 60 80 100 120 140 160 180 200 220
Residue Number
B
Mg° Zn°
Mg* Zn°
0.6
0.5
0.4
0.3
0.2
0.1
0
0 20 40 60 80 100 120 140 160 180 200 220
Residue Number
C
Mg° Zn°
Mg* Zn*
0.6
0.5
0.4
0.3
0.2
0.1
0
0 20 40 60 80 100 120 140 160 180 200 220
Residue Number

Fig. 3.

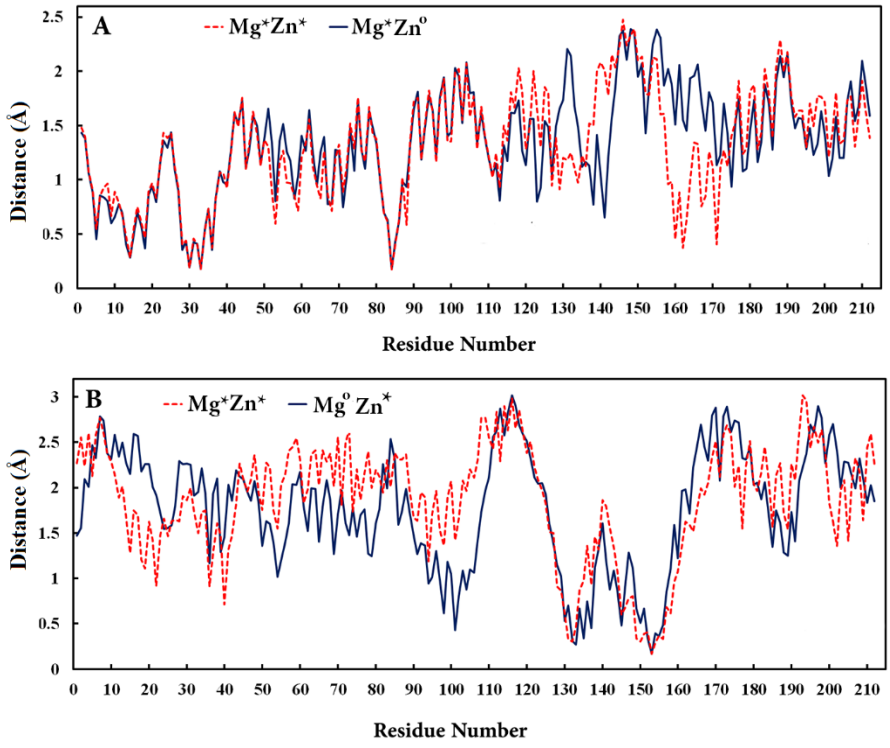
A
Mg*Zn*
Mg*Zn°
Distance (Å)
Residue Number
B
Mg*Zn*
Mg° Zn*
Distance (Å)
Residue Number

Fig. 4.